Shaping the light transmission through a multimode optical fibre: complex transformation analysis and applications in biophotonics

Tomáš Čižmár[1,*] **and Kishan Dholakia**[2]

[1]*School of Medicine, University of St Andrews, North Haugh, St Andrews, Fife, KY16 9TF, Scotland, UK*

[2]*SUPA, School of Physics & Astronomy, University of St Andrews, North Haugh, St Andrews, Fife, KY16 9SS, Scotland, UK*

[*]*tc51@st-andrews.ac.uk*

Abstract: We present a powerful approach towards full understanding of laser light propagation through multimode optical fibres and control of the light at the fibre output. Transmission of light within a multimode fibre introduces randomization of laser beam amplitude, phase and polarization. We discuss the importance of each of these factors and introduce an experimental geometry allowing full analysis of the light transmission through the multimode fibre and subsequent beam-shaping using a single spatial light modulator. We show that using this approach one can generate an arbitrary output optical field within the accessible field of view and range of spatial frequencies given by fibre core diameter and numerical aperture, respectively, that contains over 80% of the total available power. We also show that this technology has applications in biophotonics. As an example, we demonstrate the manipulation of colloidal microparticles.

OCIS codes: (060.2350) Fiber optics imaging; (090.1760) Computer holography; (090.1000) Aberration compensation; (170.4520) Optical confinement and manipulation.

References and links

1. I. M. Vellekoop and A. P. Mosk, "Focusing coherent light through opaque strongly scattering media," Opt. Lett. **32**, 2309–2311 (2007).
2. I. M. Vellekoop and A. P. Mosk, "Phase control algorithms for focusing light through turbid media," Opt. Commun. **281**, 3071–3080 (2008).
3. I. M. Vellekoop, E. G. van Putten, A. Lagendijk, and A. P. Mosk, "Demixing light paths inside disordered metamaterials," Opt. Express **16**, 67–80 (2008).
4. I. M. Vellekoop and A. P. Mosk, "Universal optimal transmission of light through disordered materials," Phys. Rev. Lett. **101**, 120601 (2008).
5. T. Čižmár, M. Mazilu, and K. Dholakia, "In situ wavefront correction and its application to micromanipulation," Nat. Photonics **4**, 388–394 (2010).
6. A. J. Thompson, C. Paterson, M. A. A. Neil, C. Dunsby, and P. M. W. French, "Adaptive phase compensation for ultracompact laser scanning endomicroscopy," Opt. Lett. **36**, 1707–1709 (2011).
7. M. Paurisse, M. Hanna, F. Druon, P. Georges, C. Bellanger, A. Brignon, and J. P. Huignard, "Phase and amplitude control of a multimode lma fiber beam by use of digital holography," Opt. Express **17**, 13000–13008 (2009).
8. R. D. Leonardo and S. Bianchi, "Hologram transmission through multi-mode optical fibers," Opt. Express **19**, 247–254 (2011).
9. R. Gerchberg and W. Saxton, "A practical algorithm for the determination of the phase from image and diffraction plane pictures," Optik **35**, 237–246 (1972).

#150802 - $15.00 USD Received 11 Jul 2011; revised 15 Aug 2011; accepted 21 Aug 2011; published 14 Sep 2011

10. T. Čižmár and K. Dholakia, "Tunable Bessel light modes: engineering the axial propagation," Opt. Express **17**, 15558–15570 (2009).
11. G. Z. Yang, B. Z. Dong, B. Y. Gu, J. Y. Zhuang, and O. K. Ersoy, "Gerchberg–Saxton and Yang–Gu algorithms for phase retrieval in a nonunitary transform system: a comparison," Appl. Opt. **33**, 209–218 (1994).
12. K. Dholakia and T. Čižmár, "Shaping the future of manipulation," Nat. Photonics **5**, 335–342 (2011).
13. A. Ashkin, "Acceleration and trapping of particles by radiation pressure," Phys. Rev. Lett. **24**, 156–159 (1970).
14. A. Ashkin, J. M. Dziedzic, J. E. Bjorkholm, and S. Chu, "Observation of a single-beam gradient force optical trap for dielectric particles," Opt. Lett. **11**, 288–290 (1986).
15. C. Liberale, P. Minzioni, F. Bragheri, F. De Angelis, E. Di Fabrizio, and I. Cristiani, "Miniaturized all-fibre probe for three-dimensional optical trapping and manipulation," Nat. Photonics **1**, 723–727 (2007).
16. W. Wadsworth, R. Percival, G. Bouwmans, J. Knight, T. Birks, T. Hedley, and P. S. Russell, "Very high numerical aperture fibers," Photon. Technol. Lett. **16**, 843–845 (2004).
17. P. J. Rodrigo, V. R. Daria, and J. Glückstad, "Real-time three-dimensional optical micromanipulation of multiple particlesand living cells," Opt. Lett. **29**, 2270–2272 (2004).
18. T. Čižmár, O. Brzobohatý, K. Dholakia, and P. Zemánek, "The holographic optical micro-manipulation system based on counter-propagating beams," Laser Phys. Lett. **8**, 50–56 (2011).
19. A. Constable and J. Kim, "Demonstration of a fiber-optical light-force trap," Opt. Lett. **18**, 1867–1869 (1993).
20. J. Guck, R. Ananthakrishnan, H. Mahmood, T. Moon, C. Cunningham, and J. Kas, "The optical stretcher: a novel laser tool to micromanipulate cells," Biophys. J. **81**, 767–784 (2001).
21. M. Pitzek, R. Steiger, G. Thalhammer, S. Bernet, and M. Ritsch-Marte, "Optical mirror trap with a large field of view," Opt. Express **17**, 19414–19423 (2009).
22. R. Di Leonardo, F. Ianni, and G. Ruocco, "Computer generation of optimal holograms for optical trap arrays," Opt. Express **15**, 1913–1922 (2007).

1. Introduction

The randomization of laser light in various media presents a substantial obstacle for the exploitation of photonics in many scientific disciplines including biology and medicine. Recently it has been demonstrated that with the use of use of a dynamic diffractive optical elements, namely the spatial light modulator (SLM), one can overcome such degradation by carefully pre-shaping the beam in phase prior to its entry to a randomizing medium. The shaped field modulation in this form cancels all the aberrations that the beam collects propagating through the randomizing object [1–4]. An alternative approach allowing complex optimization, that is in both phase and amplitude, was introduced in 2010 [5] showing the first application of this technology in the field of optical manipulation where trapping through turbid media was demonstrated. This opens up the additional prospect of allowing photonics to penetrate deeper in imaging and enhancing therapeutic applications. The potential application of this generic technique for optimizing throughput of optical fibres was also suggested [5] but not expanded upon. In contrast to highly scattering and diffusive media (e.g. biological tissues) where the principal source of randomization is light scattering, a multimode fibre represents a system where the light randomization results mainly from unpredictable phase delays between individual propagating modes as well as the coupling of light between modes.

The numerous diverse applications of single mode fibre technology is not without its limitations. Rectifying the light propagation within a multimode optical fibres would have a huge impact in many disciplines particularly those related to photonics applications within the life sciences. In particular the last decade has seen the emergence of a suite of fibre based technologies in imaging, manipulation and nanosurgery that may all benefit from the usage of multimode fibre technology. Endoscopic techniques have come to the fore and there is a burgeoning need for optimal fibre technology to deliver light both *in vitro* and *in vivo* in a controlled fashion [6]. Thus the ability to control the output profile of a multimode fibre offers unprecedented opportunities.

In this paper we show that exploiting and advancing the method presented in [5] we can fully analyze the light transformation of an optical system containing a multimode optical fibre. This analysis is between input modes represented in our case by considering sub-domains at the

#150802 - $15.00 USD Received 11 Jul 2011; revised 15 Aug 2011; accepted 21 Aug 2011; published 14 Sep 2011

SLM plane and the output modes - optimally focused beams at the output fibre facet taking into account all of the parameters of the field i.e. the phase, amplitude and polarization distributions. Once the system transformation is acquired we can control (shape) the output light at will.

Controlling the output of a multimode fibre with the use of a computer generated hologram has been previously attempted. Amplitude and phase correction was demonstrated for a large mode area fibre that allowed four propagating modes [7]. Di Leonardo and Bianchi presented a direct search method based approach to concentrate the multimode fibre output light into one or several spots [8]. Our approach is a major advancement upon these techniques and presents a method to acquire full information about light randomization within the fibre and the subsequent maximization of the available optical power. We show that in contrast to the case of [8], where no amplitude nor polarization of transmitted light was analyzed, we retain the equivalent amount of total available power while splitting the light between several focal points. We also show that with the employment of an alternative form of the Gerchberg-Saxton algorithm [9], we can form arbitrary amplitude distributions at the fibre facet retaining almost all of the available optical power. Finally, we present an application of these approaches for one area in biophotonics, namely optical manipulation. We show the confinement and manipulation of a number of microparticles using the output field of the multimode fibre.

The paper is organized as follows: firstly, the principles of the optimization method are explained and the experimental geometry and its capabilities are both introduced. Then we progress to discuss focussing of the output light into single focal points that form a representation in which any output field can be expressed. In the subsequent sections, we show how the total power can be split between a number of these base modes with no power losses. We demonstrate the generation of an arbitrary intensity distribution at the fibre output and conclude with the experimental application of our method in the field of optical manipulation.

2. Principles

As demonstrated elsewhere [5] the optimization algorithm used here is based on a decomposition of the initial laser field at the SLM plane into a series of orthogonal modes each corresponding to a different square region (sub-domain) of the SLM. Modulating a particular mode with a blazed phase grating one can transfer the mode in a Fourier plane from its original location in the 0^{th} order area into the 1^{st} order as shown in figures 1a and 1b. This is equivalent to turning the modes 'on' or 'off' as only light propagating into the 1^{st} order area is coupled into the optical fibre. One such mode is selected as a reference and all the remaining modes are examined one by one as follows. A mode under 'test' (f_t), together with a reference mode (f_r), propagates through the optical system. They interfere in the destination plane (output fibre facet, see figure 1c) giving an intensity signal that is observed by an intensity probe (single pixel of a CCD camera). From the intensity evolution ($I(p)$ - see fig. 1d) recorded by the intensity probe while altering the phase of a tested mode (p - see bottom of figure 1a) we can extract both the optimal phase ψ_t, giving the highest intensity at the probe, as well as the amplitude of the tested mode $|f_t|$. Repeating this procedure for all the input modes and then turning them 'on' simultaneously with the optimal phase results in optimum focussing of the signal at the intensity probe as all the modes carrying the entire optical power will interfere constructively. As we shall explain later, the amplitude signal is not irrelevant and in a number of cases provides extremely valuable information. It is worth remarking that the CCD presents an array of independent intensity probes - pixels. The focussing optimization for all of these pixels may be achieved simultaneously within one full execution of the optimization procedure.

One may assume that the complete series of amplitude and phase modulation for every point at the fibre output facet represents a systematic orthogonal transformation between the input field at the SLM plane and the output field of the fibre. This can be expressed in the representa-

#150802 - $15.00 USD Received 11 Jul 2011; revised 15 Aug 2011; accepted 21 Aug 2011; published 14 Sep 2011

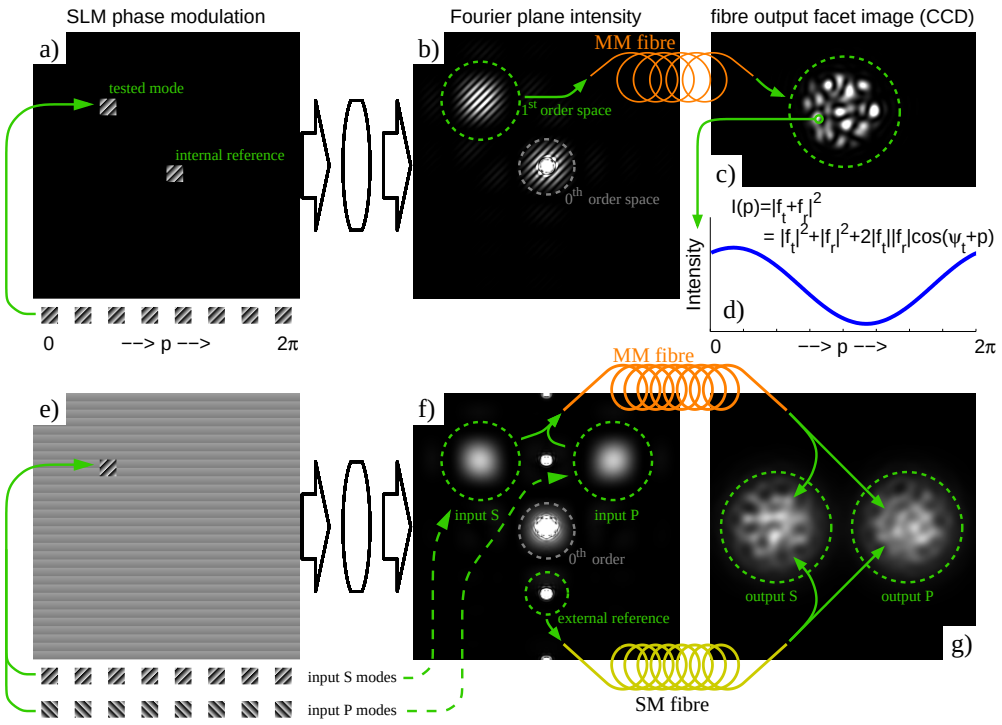

Fig. 1. Principle of the optimization procedure. a-d - standard method [5] applied for the optimization of multimode optical fibre; e-g - enhanced approach allowing full systematic transformation analysis including phase, amplitude and polarization. Using an external reference eliminates problem with 'blind spots' and crucially provides the missing phase and polarization calibration of output modes.

tion of optimized foci. In the original form however there are a number of obstacles standing in the way of this goal. Most importantly, it is not only the phase and the amplitude, but also the polarization of the light that is randomized within the fibre. Without polarization control one can only employ 50% of the available optical power as the remaining light is randomly spread over the output area.

Using the reference mode signal as described above inherently has several very important problems. As the reference signal propagates inside the multimode fibre, its phase and polarization is randomized before it reaches the fibre output and therefore both the resultant phase and polarization of the output modes (optimized foci) are also unknown. Finally at the fibre output this internal (or common pathway) reference mode will exhibit a speckled character with an exponential distribution of the output intensity and some parts of the fibre output will be very strongly illuminated whilst others may carry extremely low signals (see figure 1c), so termed 'blind spots', where the optimization cannot be performed due to the lack of reference signal. One would therefore need a very large dynamic range and resolution of the intensity detector used to cover the whole spectrum of signal levels. This would however only minimize the problem as due to the inherent statistical nature of this issue, it cannot be completely eliminated.

Here we show that all these problems may be addressed within an experimental geometry having solely one SLM and one CCD camera. The principles are summarized in fig. 1e-g.

#150802 - $15.00 USD Received 11 Jul 2011; revised 15 Aug 2011; accepted 21 Aug 2011; published 14 Sep 2011

We use three different optical pathways that are separated in Fourier space - two for each polarization of the input modes and one that acts as an external reference. Light from any part of the SLM can be sent to each of the three pathways by applying the appropriate blazed phase grating. Instead of an internal reference mode, we use a fraction of the previously unused optical power separated from the zeroth order using a further blazed phase grating (but with a different orientation than that for the tested modes) that allows us to control its amplitude and phase. The reference light is then coupled to a single mode optical fibre that delivers this signal separately to the detector. The light has the form of a collimated Gaussian beam with a very uniform intensity distribution over an area exceeding the output fibre image and has a flat wavefront, thus eliminating problems with randomization of the internal reference. Losing the advantage of a common optical pathway, the feasibility to control the phase of the reference is essential in our experimental conditions as it allows us to compensate for mechanical and thermal drift of the setup within a feedback loop that keeps the phase relation between the individual optical pathways stationary. Individual input modes can be sent to multimode optical fibre in both polarization states S and P. This is determined by the blazed grating used as shown in fig 1e and f. S and P input pathways are separated in the Fourier plane and the polarization of the S arm is rotated by 90° before coupling into the fibre. Finally, as there are no correlations between the polarization states of the input and output modes, optimization is performed separately for both output polarization states to capture the full parameter space of the optical transformation.

3. Experimental geometry

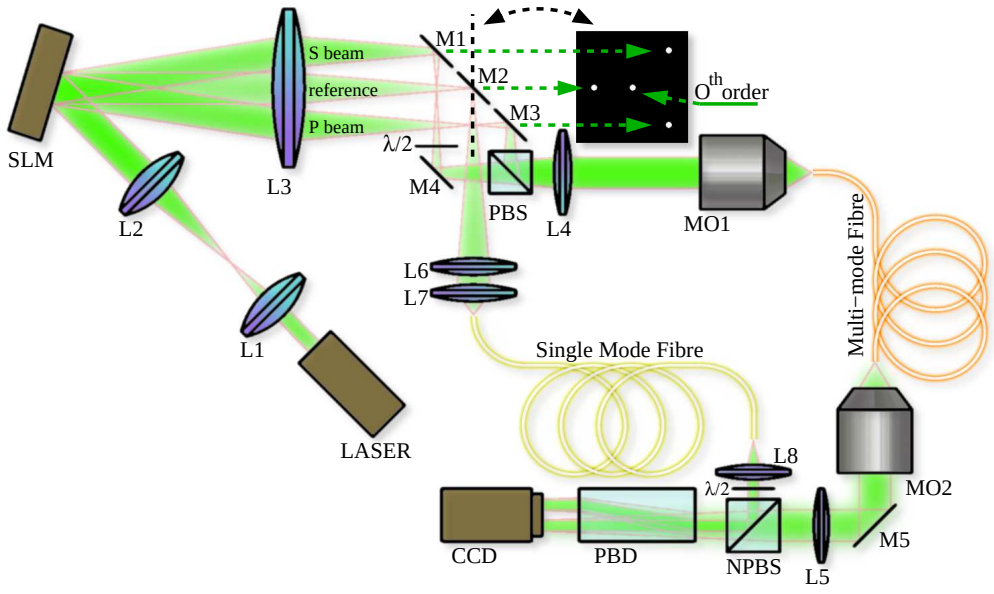

Fig. 2. The experimental geometry allowing generating of individual input modes in both polarization states and feedback loop stabilizing the phase relation between multimode optical fibre path and the external reference pathway. L1-L8 - lenses, M1-M5 - mirrors, PBS - polarizing beam-splitter, NPBS - non-polarizing beam-splitter, PBD - polarizing beam displacer, $\lambda/2$ - half-wave plates, MO1 and MO2 - microscope objectives.

Figure 2 shows the geometry used in our experiments. It directly reflects the above explained principles but retains the possibility to use the optimization method in its basic form [5]. We can independently add or subtract each aspect of the correction thus demonstrating the im-

#150802 - $15.00 USD Received 11 Jul 2011; revised 15 Aug 2011; accepted 21 Aug 2011; published 14 Sep 2011

portance of each parameter if needed. Single-frequency, near infrared linearly polarized light (IPG YLR-10-1064-LP-SF wavelength =1064nm) is expanded by a telescope (lens L1, f= 150 mm and lens L2, f= 300 mm) and directed onto an SLM chip. Our geometry uses a very high refresh-rate SLM device exceeding 100 Hz (BNS P512-1064) with a resolution of 512×512 pixels. The SLM area is split into 4096 sub-domains, each of 8×8 pixels that individually represent the input modes. Due to the high SLM refresh-rate, the optimization for all the modes in both input polarization states and with the feedback takes less than one hour. If the CCD can be synchronized with SLM, the optimisation time would be reduced by 50%. The S and P polarisation pathways are separated in the Fourier plane of the lens L3 (f=400 mm) by mirrors M1 and M3. The polarization of the S-pathway is rotated by 90° and merged with P by polarizing beam-splitter PBS. Both paths are then coupled into the multimode fibre by a telescope formed by lens L4 (f=200 mm) and microscope objective MO1 (Mitutoyo M Plan Apo 20x 0.42 NA) in such a way that the S and P fractions of the SLM Fourier plane are overlapped and imaged onto the input facet of the fibre. The multimode fibre (Thorlabs M14L01) has core diameter of 50 μm and cladding diameter of 125 μm, with NA of 0.22. This allows approximately 400 propagating modes. The length of the fibre used is 1 m. We remark that this is more than sufficient for future micro-fluidic chip or micro-endoscopy applications. Apart from the requirements on laser performance (narrow bandwidth of $<$ 100 kHz and wavelength stability), we are not aware of any fundamental detriment to the use of longer fibre lengths with our method. The multimode fibre output facet is imaged on the CCD chip (Basler pi640-210gm) by a microscope objective MO2 (Newport M 20x, 0.40 NA) and a tube lens L5 (f=200 mm). The reference light signal is separated from the Fourier plane by mirror M2 and coupled into the single-mode optical fibre (Thorlabs p3-830A-FC-2) by lenses L6 (f=200 mm) and L7 (aspherical f=15 mm, NA=0.5). At the fibre output, the beam is collimated by lens L8 (aspherical, f=8 mm) and merged with the multimode fibre pathway at non-polarizing beam-splitter NPBS. Before all the signals reach the CCD plane, the S and P output polarization states are separated by passage of the beam through a polarizing beam displacer creating two images at separate regions of the CCD.

4. Generating individual output modes

The previous two sections explained how we can analyze the entire field transformation of the system with a multimode optical fibre between input modes represented by SLM sub-domains and output modes represented by series of optimized foci. The transformation is given by four modulation functions (phase and amplitude for each input polarization) of all 64×64 input modes for every output mode. During the optimization process we analyzed the intensity signal from 120x120 pixels for each of the two output polarizations so the transformation contains $\approx$0.5Gb of information in an unsigned 8-bit representation of the data. Mathematically, we can express the transformation by 6 indexes as $T^{u,v,w}_{k,l,m}$ where k and l are the position indexes of the input modes with possible values between 1 and 64, m is the polarization of the input modes with two values of S and P, u and v are the position indexes of the output modes with values between 1 and 120 and w is the polarization of the output modes also with two values of S and P. The transformation is complex: $T^{u,v,w}_{k,l,m} = A^{u,v,w}_{k,l,m}\cdot e^{\left[i\cdot P^{u,v,w}_{k,l,m}\right]}$, where the amplitude $A^{u,v,w}_{k,l,m}$ is a real positive array, and the phase $P^{u,v,w}_{k,l,m}$ is has real values from interval $\langle-\pi,\pi\rangle$. An example of the system transformation for a single output mode $(u,v,w)=(30,30,s)$ is shown in figure 3.

We now discuss how the same experimental geometry introduced in fig. 2 can be used to generate individual output modes, combine them and generate complex output fields.

In the ideal case, a single output mode would be generated optimally (containing 100% of the available optical power) when all the analyzed input modes are coupled into the fibre with the appropriate amplitude, phase and polarization. During the optimization procedure, the field at

#150802 - $15.00 USD Received 11 Jul 2011; revised 15 Aug 2011; accepted 21 Aug 2011; published 14 Sep 2011

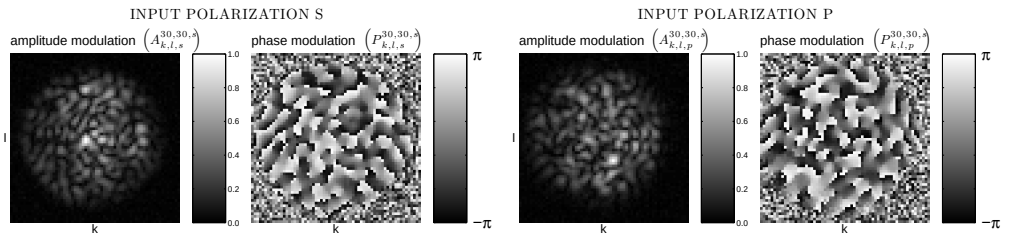

Fig. 3. Example of modulation functions corresponding to single output mode. These functions are results of the optimization procedure analyzing intensity signal for one CCD pixel. The complex transformation contains a series of such four functions for every output mode.

the input SLM plane has only a single polarization and the polarization control of input modes was achieved by applying a different blazed grating G_s and G_p. This also has to be applied when the SLM modulation function $M^{u,v,w}_{k,l}$ for generating output modes is designed and may be considered as:

$$M^{u,v,w}_{k,l} = A^{u,v,w}_{k,l,s} \cdot e^{\left[i\cdot\left(P^{u,v,w}_{k,l,s}+G_s\right)\right]} + A^{u,v,w}_{k,l,p} \cdot e^{\left[i\cdot\left(P^{u,v,w}_{k,l,p}+G_p\right)\right]}. \tag{1}$$

For a better understanding, the modulation for the output mode $(u,v,w) = (30,30,s)$ can be demonstrated in an image form (selection of only 16×16 input modes) as follows:

$$M^{30,30,s}_{k,l} = \left(\text{amplitude}\right)\cdot e^{\left(i\cdot\left(\text{phase} + \text{ramp}\right)\right)} + \left(\text{amplitude}\right)\cdot e^{\left(i\cdot\left(\text{phase} + \text{ramp}\right)\right)}$$
$$= \left(\text{amplitude}\right)\cdot e^{\left(i\cdot\left(\text{phase}\right)\right)}. \tag{2}$$

In the following text, this will be referred to as a 'complex superposition of input polarizations'. For each output mode the required SLM modulation has both phase and amplitude distributions. When designing the SLM modulations, there is no doubt that the phase transformation $P^{u,v,w}_{k,l,m}$ is indeed essential and when missing, the light output is entirely randomized. If the input polarization information is absent, i.e. the input modes are only coupled in one polarization state:

$$M^{u,v,w}_{k,l} = A^{u,v,w}_{k,l,s} \cdot e^{\left[i\cdot\left(P^{u,v,w}_{k,l,s}+G_s\right)\right]}, \tag{3}$$

on average, we lose control over 50% of the available power (only 50% of input modes would constructively interfere at the selected point, reducing the intensity to 25% , but the used 50% of modes carries all of the available power - i.e. their intensity is doubled). The remaining power is randomly spread between other output modes. If the amplitude modulation is not used, that is all the modes are coupled into the fibre with a constant amplitude, it can be shown that for a very large number of modes propagating in the system, the power efficiency drops to a value of $\frac{\pi}{4}$ i.e.

#150802 - $15.00 USD Received 11 Jul 2011; revised 15 Aug 2011; accepted 21 Aug 2011; published 14 Sep 2011

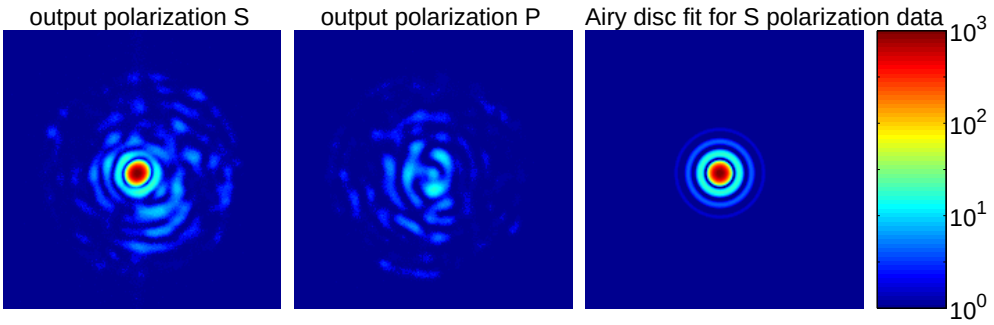

Fig. 4. Example of an output mode generated within the experimental geometry. The mode for $(u,v,w) = (60,60,s)$ was recorded by CCD while applying phase only modulation $\arg\left[M_{k,l}^{60,60,s}\right]$ at the SLM, where $M_{k,l}^{60,60,s}$ was designed following equation 1. We show both CCD output polarization regions as well as the optimal fit with the expected intensity distribution of Airy disc.

$\approx 78.5\%$ with the remaining $\approx 21.5\%$ of power randomly spread over other output modes. As the number of modes allowed to propagate within our multimode fibre is limited to ≈ 400, we can expect variations of the efficiency around the value of $\frac{\pi}{4}$ with a standard deviation of 2%. If one would however attempt to perform amplitude modulation with a uniformly illuminated SLM (this is possible even on phase only modulators, see e.g. [10]), the power losses will be many times higher, as the amplitude modulation (see fig. 3) will also have a speckled nature and one would need to sacrifice a large amount of the power producing input modes with low amplitude to be able to produce high intensity modes, thus reducing the overall power efficiency to only a few percent. Therefore, in this study, we do not introduce any amplitude modulation for the input modes, and employ only the phase - $\arg\left[M_{k,l}^{u,v,w}\right]$ at the SLM. However we stress that if further reduction of the random background signal is essential, amplitude modulation would bring better results.

Let us also remark, that even if amplitude modulation is not applied to the SLM, the amplitude component of systematic transformation $A_{k,l,m}^{u,v,w}$ is still of relevance. If this was not available, the SLM modulations would be designed as:

$$M_{k,l}^{u,v,w} = e^{\left[i\cdot\left(P_{k,l,s}^{u,v,w}+G_s\right)\right]} + e^{\left[i\cdot\left(P_{k,l,p}^{u,v,w}+G_p\right)\right]}, \tag{4}$$

that will be referred to as 'phase only superposition of input polarizations', and, as we shall demonstrate experimentally (Appendix A and B), this has a considerably lower efficiency when compared to the 'complex superposition of input polarizations' (equation 1) described.

Figure 4 shows an example of a generated output mode using the complex superposition of input polarizations (equation 1) . The image data were obtained by merging several CCD frames taken at various exposure times as we were unable to cover all the signal levels with an 8-bit detector. We fitted the measured data for 100 different output modes with an expected Airy disc profile (5 parameter function - center x, center y, amplitude, central core diameter and offset) finding that they carry in average 83% of the total power transmitted by the fibre with a standard deviation of 3%. This is in a good agreement with the value of $\frac{\pi}{4}$, ($\approx 78.5\%$) discussed earlier, the difference is probably caused by a small non-linear response of the CCD camera at different exposure times. The radius of the fitted spot corresponds to value of numerical aperture equal to $NA = 0.18$, that is about 20% smaller compared with value 0.22 given by fibre manufacturer. This may be caused by Gaussian illumination of SLM, thus reducing intensity of modes with

#150802 - $15.00 USD Received 11 Jul 2011; revised 15 Aug 2011; accepted 21 Aug 2011; published 14 Sep 2011

higher radial coordinates.

Appendix A (figures 8 and 9) presents the overall statistics of single output mode generation using all the discussed approaches. It demonstrates, that with the use of external reference, we can eliminate the problematic issue of 'blind spots' and that with the use of both polarization we can double the output mode intensities for the same optical power in the system and enhance the signal/noise ratio by a factor in excess of 6. It also shows that complex superposition of input polarizations yields more than 20% higher intensities of the output modes compared to the phase only alternative.

5. Simultaneous generation of multiple output modes

In this section we show how the available power can be split to simultaneously generate the required number of output modes. Similarly as in the case of combining polarizations, we can use a complex superposition of modulations obtained from equation 1 corresponding to individual modes:

$$M_{k,l}^{N} = \sum_{q=1}^{N} \sqrt{a_q} \cdot M_{k,l}^{u_q, v_q, w_q}, \tag{5}$$

where N is the number of output modes. The required output modes are indexed by variable q and a_q are required intensity contributions of the composition of output modes. Again, if amplitude modulations are not available one can proceed with phase only superposition of output modes:

$$M_{k,l}^{N} = \sum_{q=1}^{N} \sqrt{a_q} \cdot e^{i \cdot \arg\left[M_{k,l}^{u_q, v_q, w_q}\right]}. \tag{6}$$

This case was extensively studied in [8] for the case of two output modes, showing significant deviations of power distribution between individual points as well as $\approx 20\%$ of efficiency decrease in case of equally distributed optical power between the modes. We address this issue in Appendix B (figure 10). Our experimental results show that when complex superposition of output modes is used, there are no power losses and intensity is distributed between the individual spots as required.

Power splitting into larger number of output modes is demonstrated in figure 5 where individual output modes are combined by both the complex superposition as well as by the use of an Gerchberg-Saxton (GS) algorithm [9] alternative for the case of the non-unitary systematic transformation [11] (see Appendix C). This combines individual output modes with phases, such that the resulting SLM modulation has the most uniform amplitude distribution. Let us stress that the G-S algorithm is a purely mathematical procedure and no hardware feedback is essential to optimize the results.

As we generate larger numbers of output modes, they will cover significant fraction of the fibre output area and the unused portion of light that is randomly spread starts to contribute to the intensity of individual modes that will manifest themselves as higher intensities there. The data shown in figure 5 were corrected by removing the random signal intensity contributions. As can be seen in figure 5, the G-S algorithm leads to larger efficiency (9% on average), a more uniform distribution of power between individual output modes and power efficiency exceeding 90%.

6. Generation of arbitrary intensity distributions

The fibre we use allows only about 400 propagating modes, while we use $2 \times 64 \times 64$ input and $2 \times 120 \times 120$ output modes to describe the systematic transformation. Hence the transformation is highly over-sampled and not-unitary. This is not an issue in any of the applications

#150802 - $15.00 USD Received 11 Jul 2011; revised 15 Aug 2011; accepted 21 Aug 2011; published 14 Sep 2011

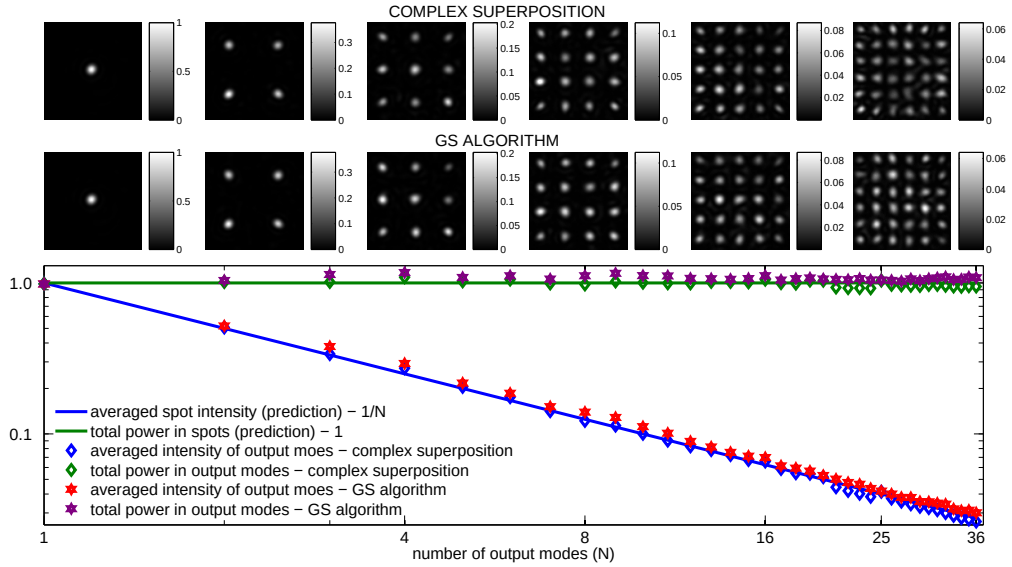

Fig. 5. Simultaneous generation of output modes by complex superposition and G-S algorithm. Top: CCD frames showing different numbers of modes. Bottom: total power in output modes and averaged power per mode for the cases of complex superposition and G-S algorithm. Solid lines show the expected behaviour, considering that the total power distributed between individual modes is conserved.

demonstrated in this paper, but for the purposes of more advanced beam shaping (e.g. generation of an optical vortex) the issue of orthogonality between individual input modes and most importantly, the output modes would need to be addressed. When the output modes are generated in very close proximity to each other, they start to influence themselves by unwanted interference effects. The G-S algorithm is however, very useful in these cases, as these interference effects are very strongly suppressed and arbitrary intensity distributions can be generated at the fibre output with very high quality as demonstrated in figure 6.

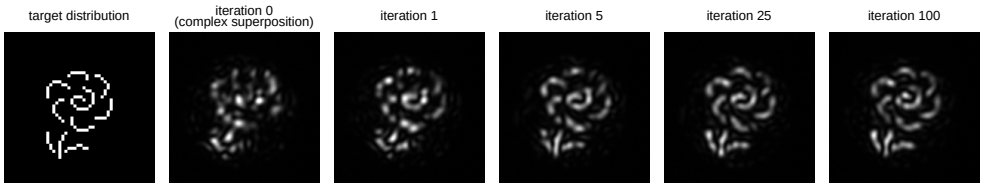

Fig. 6. G-S algorithm based beam shaping of the output of a multimode fibre. The target distribution is formed by modes with minimal mutual distance of 4 CCD pixels, that corresponds to 2.7 μm at fibre output facet, or 0.2$\times$ the size of the measured output mode diameter (central core of the fitted Airy disk). Output modes are strongly influenced by unwanted interference effects when combined by complex superposition (equation 5) - iteration 0. The G-S algorithm gradually improves the amplitude distribution as it converges after around 100 iterations. Results for every iteration are presented in (Media 1).

#150802 - $15.00 USD Received 11 Jul 2011; revised 15 Aug 2011; accepted 21 Aug 2011; published 14 Sep 2011

7. Application for optical manipulation

In this section we demonstrate application of optimized output modes to optical manipulation [12] as a key area in the broader topic of biophotonics. As the output modes form a series of optimally focussed light beams, they will attract high refractive index objects from their vicinity via the gradient force, as identified by Ashkin [13] four decades ago. The numerical aperture of the output modes in our geometry is too low to allow stable 3-D confinement of micron-size objects by means of optical tweezers [14] as the axial gradient force cannot counter-balance radiation pressure. It was however, demonstrated, that micro-structured optical fibres are capable of 3-D optical trapping [15]. The availability of high NA multimode photonic crystal fibres [16] ($NA > 0.9$) may allow novel fibre-based geometries for 3-D holographic multiple optical tweezers employing our optimization algorithms.

In low NA systems, 3-D confinement can be achieved by introducing a pair of counter-propagating output modes for every optical trap [13, 17, 18]. Using optimized multimode fibres in a counter-propagating geometry would represent major advance for this very popular fibre-trap geometry [19, 20]. Elegantly, one can also achieve 3-D trapping in single-fibre geometry introducing pairs of beams in two distinct axial planes and reflecting them against each other by a mirror [21]. This would be particularly suitable for our case as fibre facet needs to be accessible during the optimization procedure.

In this paper, however, we demonstrate simple case of 2-D manipulation only, where trapped particles are confined and positioned at the interface of liquid sample medium and glass coverslip. To provide illumination of particles, white light was coupled into the multimode fibre using a dichroic mirror placed between lens L4 and microscope objective MO1 (see fig. 2). The optimization procedure was repeated with the image plane of the observational objective MO2 moved 15 μm away from the fibre facet to allow enough space for access of particles and manipulation. The immobilized fibre output was submerged into the liquid sample (de-ionized water) containing polymer microparticles, each $3\mu m$ in diameter. The laser light was blocked by a dichroic filter placed before CCD, allowing transmission of the white-light signal. In the example shown in fig. 7 and (Media 2), particles were confined in the static intensity pattern formed by complex superposition of output modes and sequentially moved by applying pre-calculated SLM modulation masks corresponding to different arrangements of the output modes.

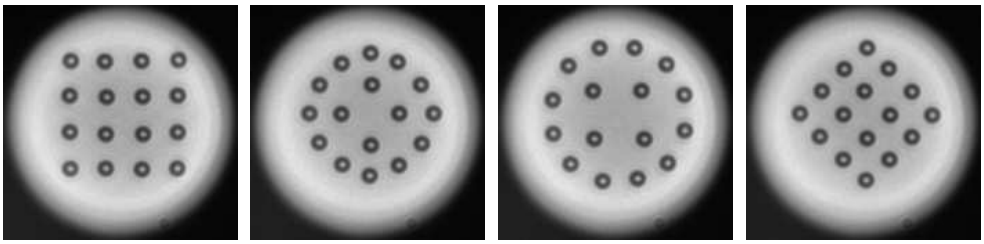

Fig. 7. 2-D optical manipulation of 16 polystyrene micro-particles each of $3\mu m$ in diameter. Both the trapping beams (output modes) and the white-light illumination are delivered by the multimode optical fibre. See also (Media 2), that is $3\times$ faster than real-time.

8. Conclusion

In this paper we have introduced a powerful approach allowing complex quantification of light propagation through multimode optical fibres and its control using a spatial light modulator. By

#150802 - $15.00 USD Received 11 Jul 2011; revised 15 Aug 2011; accepted 21 Aug 2011; published 14 Sep 2011

applying this technique, the light transformation between the input and output modes can be fully analyzed for all parameters i.e. phase, amplitude and polarization. The study presents a major step towards novel exploitation of multimode optical fibres in many disciplines. We also show control of the output light with maximal efficiency, utilizing over 80% of the available optical power in a form of single output mode (focussed beam), multiple foci or more elaborate intensity profiles. We have employed this system for the first demonstrations in this instance of optical trapping. We have presented simultaneous confinement and manipulation of a large number of high index particles. Future work will involve a more systematic exploration of these possibilities towards micro-endoscopy and lab-on-a-chip applications, including 3-D optical manipulation.

Appendix

A *Evaluation of discussed approaches for generating individual output modes*

Figure 8 and 9 demonstrate the overall statistics of peak intensities corresponding to individual output modes. All the 120×120 output modes were generated one by one and their peak intensities were recorded by CCD.

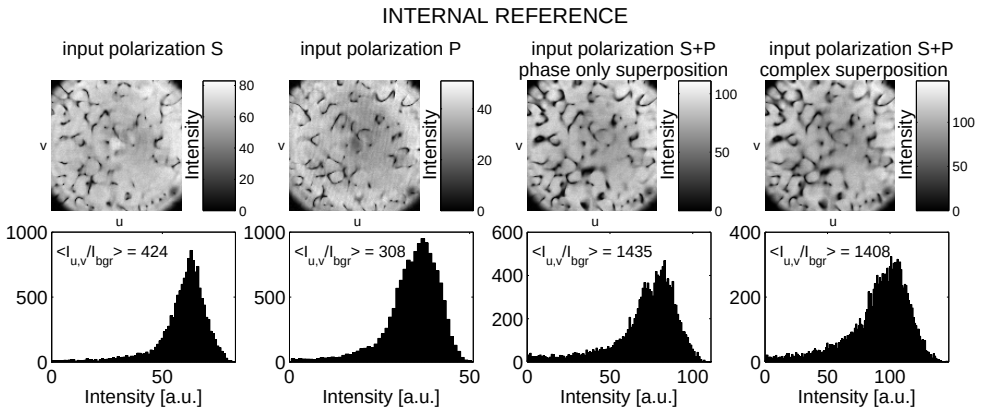

Fig. 8. Generation of output modes using internal reference mode. First two columns show output mode intensities and their histograms for single input polarizations (equation 3). The third column shows data for phase only superposition of input polarizations (equation 4). Last column shows results for complex superposition of input polarizations (equation 1).

The data are presented in a form of a bitmap where every point represents the peak intensity of particular output mode (u,v) as well as histograms of the measured values bellow. We also calculated the averaged value of ratio between the particular mode intensity and the level of surrounding intensity noise $\langle I_{u,v}/I_{bgr} \rangle$ defined in [1]. The data are only shown for one output polarization $(w = S)$, but the results for the second output polarization are very similar. First two columns show the results when single input polarizations only were used (equation 3). The third column shows output mode intensities for SLM modulation calculated by phase only superposition of input polarizations (equation 4). Finally, the last column shows results for complex superposition of input polarizations (equation 1). Here we also the take opportunity to demonstrate the importance of the external reference that was used for the results shown in the figure 9, while the results in the fig. 8 are obtained with the use of the internal reference, where the presence of the 'blind spots' is clearly visible. All the data were taken for the same laser power as well as camera settings.

#150802 - $15.00 USD Received 11 Jul 2011; revised 15 Aug 2011; accepted 21 Aug 2011; published 14 Sep 2011

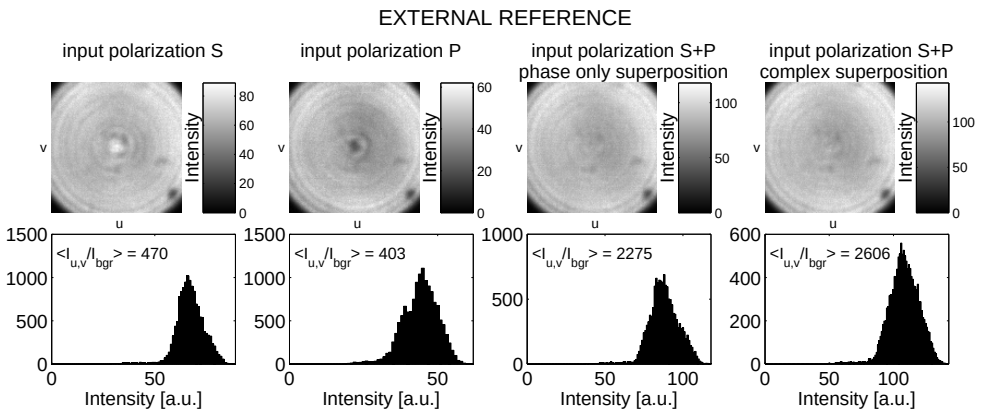

Fig. 9. Generation of output modes using external reference mode. Figure is organized the same way as fig. 8

B *Evaluation of discussed approaches for simultaneous generation of a pair of output modes*

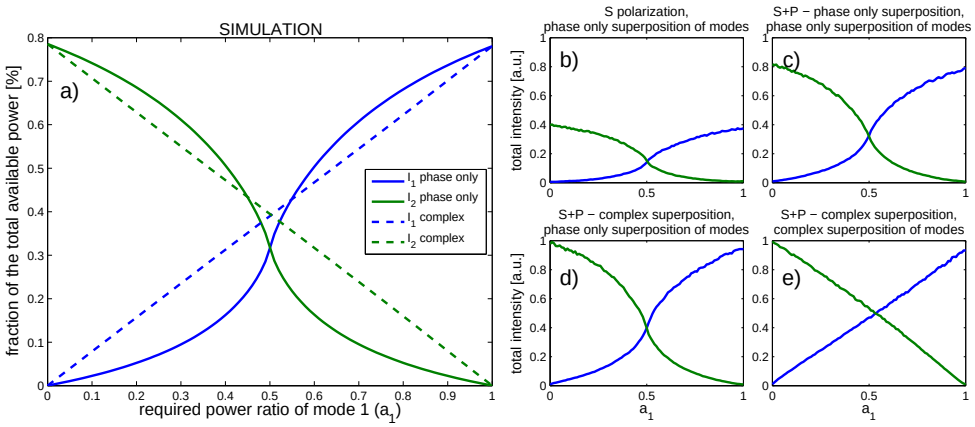

Fig. 10. Simultaneous generation of two output modes with tunable power ratio. a - numerical simulation for phase only (solid lines) and complex (dashed) superposition of output modes. Analytical functions for this dependencies are derived in [8]. b - c experimental results for the case of output modes combined by phase-only superposition (equation 6) where individual modes were generated by: b, - single polarization (equation 3); c, - phase-only superposition of input polarizations (equation 4) and d, - complex superposition of input polarizations (equation 1). Subplot d shows the optimal case of both, the input polarizations and the output modes combined by complex superposition (equations 1 and 5).

When multiple output modes are generated simultaneously without the availability of amplitude modulation for individual modes (equation 4), the resulting power ratio between the modes significantly differs from that intended [8] and the result is accompanied with power losses of up to 20%. As presented in figure 10 we observed identical behaviour for modes generated by single input polarization, phase only and complex superposition of input polarizations. This however vanishes in the case of the complex superposition of output modes (equation 5), where the power ratio between generated modes as very close to the intended one and the total power

#150802 - $15.00 USD Received 11 Jul 2011; revised 15 Aug 2011; accepted 21 Aug 2011; published 14 Sep 2011

in the pair of modes is conserved.

C *G-S algorithm alternative for the case of the systematic transformation.*

The original G-S algorithm is frequently used in Fourier systems to generate arbitrary distributions of intensities with phase only holographic modulation and while employing fast Fourier transform methods this can be very fast and efficient. If the transformation is neither Fourier nor unitary, the G-S algorithm can still be used in a form known as Yang-Gu algorithm [11]. In this paragraph we introduce this mathematical procedure using our notation. In the initial iteration, we start with the complex superposition of output modes as shown by equation 5. In every following iteration (indexed by t), we change amplitude of the SLM modulation to be uniform:

$$ {}^{t}\bar{M}^{N}_{k,l} = e^{i\cdot\arg\left[{}^{t-1}M^{N}_{k,l}\right]}, \tag{7} $$

calculate complex constitution coefficients of required output modes ${}^{t}a_q$ by a scalar product:

$$ {}^{t}c_q = \sum_{k,l} {}^{t}\bar{M}^{N}_{k,l} \cdot M^{u_q,v_q,w_q\star}_{k,l}, \tag{8} $$

re-balance their amplitudes:

$$ {}^{t}\bar{c}_q = \sqrt{a_q} \cdot e^{i\cdot\arg\left[{}^{t}c_q\right]}, \tag{9} $$

and generate a new SLM modulation:

$$ {}^{t}M^{N}_{k,l} = \sum_{q=1}^{N} {}^{t}\bar{c}_q \cdot M^{u_q,v_q,w_q}_{k,l}. \tag{10} $$

Other algorithms (e.g. weighted G-S [22]) may bring higher efficiency and uniformity for the output fields.

Acknowledgments

We thank the UK Engineering and Physical Sciences Research Council and the University of St Andrews for funding. KD is a Royal Society-Wolfson Merit Award Holder.

#150802 - $15.00 USD Received 11 Jul 2011; revised 15 Aug 2011; accepted 21 Aug 2011; published 14 Sep 2011